# Network spreading among areas: A dynamical complex network modeling approach

Qin Li, Hongkai Chen, ⓘD Yuhan Li, et al.

View Online          Export Citation          CrossMark

# Network spreading among areas: A dynamical complex network modeling approach

Qin Li,[1] Hongkai Chen,[2] Yuhan Li,[2] (ID) Minyu Feng,[2,a] (ID) and Jürgen Kurths[3]

## AFFILIATIONS

[1] School of Public Policy and Administration, Chongqing University, Chongqing 400044, People's Republic of China
[2] College of Artificial Intelligence, Southwest University, Chongqing 400715, People's Republic of China
[3] Potsdam Institute for Climate Impact Research, 14437 Potsdam, Germany

[a] Author to whom correspondence should be addressed: myfeng@swu.edu.cn

## ABSTRACT

With the outbreak of COVID-19, great loss and damage were brought to human society, making the study of epidemic spreading become a significant topic nowadays. To analyze the spread of infectious diseases among different areas, e.g., communities, cities, or countries, we construct a network, based on the epidemic model and the network coupling, whose nodes denote areas, and edges represent population migrations between two areas. Each node follows its dynamic, which describes an epidemic spreading among individuals in an area, and the node also interacts with other nodes, which indicates the spreading among different areas. By giving mathematical proof, we deduce that our model has a stable solution despite the network structure. We propose the peak infected ratio (PIR) as a property of infectious diseases in a certain area, which is not independent of the network structure. We find that increasing the population mobility or the disease infectiousness both cause higher peak infected population all over different by simulation. Furthermore, we apply our model to real-world data on COVID-19 and after properly adjusting the parameters of our model, the distribution of the peak infection ratio in different areas can be well fitted.

Published under an exclusive license by AIP Publishing. https://doi.org/10.1063/5.0102390

Network spreading dynamics is a significant issue in network science. Outbreaks of COVID-19 make research on disease transmission even more important and strategies for epidemic prevention are usually proposed from a regional level. Therefore, this paper establishes an epidemic model considering epidemic spreading among areas. In our model, a network is constructed where nodes represent areas, and edges denote migrations between two areas. For each node in the network, there is a dynamic transition among susceptible, infected, and recovered individuals. We give a proof of the stability at the final state of the system and find that the final solution is only related to the infected transition rate and recovery rate. Based on our model, we put forward the peak infected ratio as a significant index to measure the epidemic in different areas and analyze its property by simulation with statistical methods. By changing the structure of the network, we observe different properties of indexes. In addition, the influence of the connection strength of coupling between areas and the infection rate in the Susceptible-Infected-Recovered (SIR) epidemic model on the infected ratio is also investigated.

Additionally, we utilize our model to fit epidemical spreading data in the real world.

---

## I. INTRODUCTION

Since the outbreak of COVID-19 at the end of 2019, infectious disease has been a serious threat to public health all over the world. Controlling epidemic outbreaks does not only demand pharmaceutical interventions such as vaccination and antiviral drugs but also requires the implementation of public health measures, e.g., social distancing, shelter in place orders, disease surveillance, contact tracing, isolation, and quarantine.[1] Nowadays, there are more case data as well as analyses performed by scientists and researchers, which benefits the study of epidemiology.

Mathematical research on infectious diseases can be traced back to the acclaimed work of Kermack and McKendrick, which defines the modern mathematical modeling of infectious diseases, which has evolved through the years in an impressive body of

work,[2,3] whose culmination is well represented by the monumental summary of Anderson and May.[4] However, in the real world, the spreading of disease happens when one individual interacts with others, while in the SIR model, differential equations consider a homogeneous assumption, i.e., all individuals have equally the same possibility of getting infected or infecting others, causing inaccuracy in real-world situations where individuals have frozen patterns of interaction.[5]

Network theory provides a general framework for studying individual contacts in disease transmission.[6] Since the Watts–Strogatz network[7] (WS network) and the Barabási–Albert network[8] (BA network) were proposed, complex networks have attracted much attention from researchers and have been a useful tool in various fields. With the network theory, more models for epidemic spreading were proposed considering the structure of connection among people. A continuous-time epidemic process with constant transition rates between compartments was described by the Markov chain theory.[5] A later study found that the impact of an epidemic is increased by a small but potentially significant amount when the contacts are random rather than regular.[9] In addition, quantitatively the numerical thresholds with theoretical predictions of the heterogeneous mean-field theory and the quenched mean-field theory were compared.[10] By establishing a queuing system, the increase and decrease of vertex degree can be described, and the spreading process on it can be analyzed in recent studies.[11,12]

Compared to the framework where each node corresponds to a single individual, a different framework considers nodes as entities where multiple individuals or particles can be located and eventually wander by moving along the links connecting the nodes, which are often framed as reaction–diffusion processes.[5] The analysis of the basic reproduction number in disease-free equilibrium provides a theoretical basis for the epidemic model.[13] Based on the reproduction number, an epidemic model is proposed to describe the dynamics of disease spread among patches due to population dispersal and a threshold between the extinction and persistence of the disease is established.[14] Influenza-like diseases models, in which the individual contacts are represented by contact networks, allow for a heterogeneous number of contacts and, thus, are more general than the classical homogeneous mixing model.[15] The metapopulation approach is introduced to describe spatially structured interacting subpopulations, such as city locations, urban areas, or geographical regions. With reaction–diffusion processes and metapopulation models in heterogeneous networks, the critical value of the transition in real topology can be analyzed.[16,17] Examples of the system are provided by mechanistic epidemic models, where particles represent people moving between different locations or by the routing of information packets in technological networks.[5]

With real-world data, general analysis of complex weighted networks can be obtained.[18] The contact network among people is found to be a strongly connected small-world-like graph while the locations graph is scale-free. Within the network simulation framework, the relative merits of several proposed mitigation strategies for disease spread can be analyzed.[19] At the same time, there is also various analysis of the transportation network based on each region. For example, the highway in Korea has a heavy tail while air and public ground transportation establish inhomogeneous systems and have power-law behaviors.[20] The railway network in China is found

to have both small-world and power-law properties.[21] The existing data show that the Indian railway network displays small-world property.[22] In general, it is reasonable to take the WS network or the BA network as the area network.

In addition to epidemic propagation dynamics on the networks, network synchronization has been studied by lots of researchers over decades focused on the synchronization phenomenon of a population of dynamically interacting units.[23] Barahona considered the generic synchronization of oscillator networks of arbitrary topology and linked the linear stability of the synchronous state to an algebraic condition of the Laplacian of the graph.[24] Pecora showed that determining the stability of the synchronous state can be done by a master stability function[25] and put forward the theory of identical or complete synchronization of identical oscillators in arbitrary networks.[26] Similar to the synchronization phenomenon, the consensus problem is analyzed and the consensus algorithm for the network is also proposed.[27]

With the complexity of real-world individuals' connections, the analysis of the whole system, which represents a country that has billions of population, like China or India turns out to be difficult. Taking the global interaction and local process into consideration, in this paper, we simulate epidemic spreading among areas with dynamic equations. In our model, we regard areas as nodes in a network, and the epidemic spreading among the population as the property of the area. The system has a certain stable point at the final state; however, the state in the intermediate process is complex though it plays an important role in the prevention of disease. Consequently, we put forward an index to describe the peak infected ratio, which describes the severity of the outbreak, and research studies on the simulation are conducted through statistical methods.

The paper is organized as follows: we present our model for epidemic spreading among areas in Sec. II. Section III presents simulation results for the model, where the influence of different parameters of the model is analyzed, and we apply our model to real-world data to give an analysis of the real-world situation. Conclusions and open problems are presented in Sec. IV.

## II. SPREADING MODEL AMONG AREAS

In the real world, epidemics spread among individuals with the population migration among different areas, which is neglected in most epidemic models. To address this issue, in this section, we utilize a spreading model among areas.

Two dynamic processes are included in our model, which are the epidemic spreading among individuals, and the epidemic spreading among areas. We describe the epidemic dynamics in an area through the SIR epidemic model and describe the spreading among areas by the network coupling. In detail, a network is constructed where each node denotes an area that is connected with other areas, and epidemics spread between areas through edges, which indicates the migration of population among areas in practical (Fig. 1). Inside an area as a node in our model, an epidemic, such as COVID-19, spreading among individuals is described via the SIR model. Epidemics also spread among different areas due to population migration, which can be regarded as the coupling in the network.
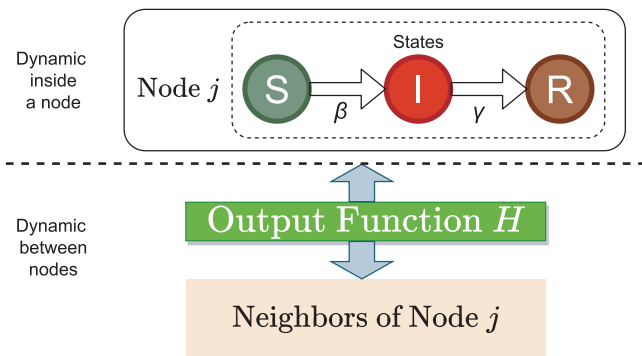
**FIG. 1.** An illustration of our area spreading network model. Node $j$ follows the SIR epidemic equations for its epidemic dynamic, where individuals transit among three states, while it interacts with its neighbors based on the output function $H$, which indicates the epidemic spreading among areas.

In general, epidemics among areas can be described as a complex dynamical network whose nodes represent different areas that have three components, including *Susceptible*, *Infected*, and *Recovered*. They stand for the ratio of the three different classes of individuals. In general, at the stable state, $I = 0$ and $R = 1 - e^{-RR_0}$, where $R_0$ is called as the basic reproduction number.

The interaction of nodes is a coupling process that can be generalized into a differential equation. In addition, different network structures describe a variety of connection patterns between areas that have different topological properties that cause the various outcomes of an epidemic. We regard the above process as the coupling of an area network, where nodes couple with each other while individuals in it follow a SIR spreading equation. Then, we define our model as follows.

In our proposed area network, a node $i$ has three states components $S_i, I_i, R_i$, following the equation below:

$$\begin{cases} \frac{dS_i}{dt} = -\beta S_i I_i - \sigma \sum_{j=1}^N H_{11} S_j, \\ \frac{dI_i}{dt} = \beta S_i I_i - \gamma I_i - \sigma \sum_{j=1}^N H_{22} I_j, \\ \frac{dR_i}{dt} = \gamma I_i - \sigma \sum_{j=1}^N H_{33} R_j, \end{cases} \quad (1)$$

where $S_i$, $I_i$, and $R_i$ denote the ratio of *Susceptible* class, *Infected* class, and *Recovered* class in the whole population and $H$ illustrates the migration rate of each class in the population. $\beta$ is the infection transition rate and $\gamma$ is the recovery transition rate. $\sigma$ is the overall connection strength between the nodes.

The motion of the node as areas (individuals inside the node), which is expressed as $\beta S_i I_i$ and $\gamma I_i$, illustrates the process of susceptible individuals getting infected, and the infected individuals getting recovered. On the other hand, $\sigma \sum_{j=k}^N H_{kk} S_j, k = 1, 2, 3$ illustrates the interaction between nodes (areas). $\sigma$ indicates the connection strength of the coupling between nodes and a higher $\sigma$ means a stronger level of interactions between nodes. The matrix $H$ illustrates the migration rate of each class in the population. For the general model, $H$ is the matrix that regulates the transformation of different states of different nodes in the interaction; however, for the simplification of the model, we confine $H$ to be diagonal. In our

model, $H_{11}$ is the migration rate of the *Susceptible* class, $H_{22}$ is the migration rate of the *Infected* class, and $H_{33}$ is the migration rate of the *Recovered* class. The higher the value in $H$, the stronger the connection of the component is, which indicates a more frequent migration of a population.

We illustrate our area spreading network model in Fig. 1. In the part *Dynamic inside a node*, we show a SIR process where the state transition is $S \to I \to R$. On the other hand, in the part *Dynamic between nodes*, the bold arrow shows the interaction between a node and its neighbors with the output function $H$. With these two parts, our model can be utilized to analyze the spreading process among the different areas. In Eq. (1), $\beta S_i I_i$ indicates the infecting process and $\gamma I_i$ indicates the recovery process. This part of the equations illustrates the SIR model, which includes $dS = -\beta SI$, $dI = \beta SI - \gamma I$, and $dR = \gamma I$, in a limited area, however. The general model divides the population into three disjoint classes of individuals, where $S$ is the *susceptible* class in which individuals contract the disease and become infected, $I$ is the *infected* class in which individuals spread the disease to the susceptible class and $R$ is the *removed* class, i.e., the class of individuals who die or recover from the disease and become immune. In addition, $\beta$ and $\gamma$ are known as the transition rates for infection and recovery, which are subject to $\beta > 0$ and $\gamma > 0$.

In detail, $\beta$ measures how fast the disease spreads among the individuals, and $\gamma$ indicates how fast individuals recur after being infected. $\beta/\gamma$ is the basic reproduction number $R_0$, and $R_0 > 1$ is the condition that the epidemic can spread.[4] When the spreading process is stationary, we have $R = 1 - e^{-\beta R/\gamma}$ and $I$ being neglected. With this equation, the process of spreading in a homogeneous population can be predicted.

In the other part of our model in Eq. (1), we propose the coupling among nodes. The item $\sigma \sum_{j=k}^N H_{kk} S_j, k = 1, 2, 3$ illustrates the coupling of different nodes through the three components. In our model, we utilize network coupling to describe the interaction among different areas, which considers the spatial effects in an epidemic. In real life, there are transportation flows or population migration between two areas all the time, consequently, the disease from one area to others via mobile population. Therefore, we take the migration process as well as the SIR process in areas into consideration. $\sigma$ is the connection strength, which indicates the degree of interaction or the frequency of migration among areas. The larger the value of $\sigma$ is, the higher degree of the interaction among areas is. In particular, our spatial model reduces to the typical SIR model, given $\sigma = 0$.

A general motion for a single node is $\dot{\mathbf{x}} = \mathbf{F}(\mathbf{x})$, where $\mathbf{x}$ is the state vector of the node in an m-dimensional space and $\mathbf{F}(\mathbf{x})$ is the dynamical equation. We assume an identical output function as $\mathbf{H}(\mathbf{x})$ for all nodes in the network and set $H(\mathbf{x}) = \mathbf{H}\mathbf{x}$, where $\mathbf{H}$ is a diagonal matrix. With the linear function, a node generates its signal and sends it to its neighbor nodes in the network, having the general coupling equation as:

**Definition 1.** A coupling equation for the proposed model is

$$\dot{\mathbf{x}}_i = \mathbf{F}(\mathbf{x_i}) - \sigma \sum_{j=1}^N G_{ij} \mathbf{H}(\mathbf{x_j}), \quad (2)$$

where $G_{ij}$ is the weight of the edge in a common network, and it is set positive to ensure that the formula is realistic.

The weight of an edge connecting two different nodes shows the strength of the connection of the area. However, to simplify the problem, we set it to be constant 1 or an unweighted network in our model, which illustrates a constant population migration strength. By restricting $G_{ii} = -\sum_{j=1, i \neq j}^{N} G_{ij}$, the adjacency matrix $G$ of the network has a zero row-sum.

Note that our stable state means that all node states are in agreement, that is, a consensus or synchronization state is reached. In this state, the epidemic can still be spreading, but all node changes will be consistent.

We next display the process of our model by components as follows:

**Spreading network among areas**

1. **Network initializing.** Randomly choose a node to be the initial area where the epidemic first outbreaks.
2. **Spreading process inside an area.** Following the SIR model, we update each state of node $j$, $(S_j, I_j, R_j)$.
3. **Spreading process among different areas.** Following the dynamical equation in Eq. (1), the state node $j$ will be coupled with nodes connected to it, implying the population migration among areas.
4. **Recording and Termination.** When the system reaches a stable state, record the state vector at every time point. We set a termination time for the whole process, the spreading process, thus, can end up by the termination time.

In this process, we first initialize the system with a given network and set all the nodes in the network having the $S$ component in the state vector to be 1, indicating there are no infected or recovered populations. Then, randomly choosing a starting node to be where the epidemic started suggests that the $I$ component of the state vector is positive. We start the epidemic process inside the area. In addition, as the disease spreads among the population in a specific area in the real world, the epidemic follows the SIR model and the infected population grows in the original area, while the infected population also gets recovered at a rate $\gamma$. With the coupling model, the disease spreads to other areas in the neighborhood as the population migration, causing the $I$ component of the state vectors of nodes connected to be positive, which leads to some individuals getting infected and then they recover after some time inside an area. As the process repeats continuously, we record the state vector at every time point. When the termination time is up, we end the process.

To better demonstrate how the model works, we illustrate an epidemic process in a network with four nodes connected in Fig. 2. The connecting nodes marked with 0, 1, 2, and 3 stand for four areas, and the labels show the ratio of the three population classes in the area they are linked to. Different colors of the node display the level of severity of the epidemic in the area by that how many populations got recovered, varying by time. The labels connected with the nodes show the value of the ratio of the three classes of the population in the node. In this process, the epidemic first started in node 0 at time $t = 0$, and we choose $t = 0, 20, 26, 33, 46$ for demonstration. In node 0, the infected first grows and then spreads to areas 1, 2, and 3. Thus,

node 0 is more likely to have the highest infected ratio during the whole period, while the other nodes go through a similar process since they are all neighbors of node 0.

From Figs. 2(a) to 2(e), the initial area gets a much more severe epidemic, while the connected areas begin to suffer the disease. In Fig. 2(a), almost all of the population are the susceptible class except a small amount of the infected population in node 0. In Fig. 2(b), the epidemic spreads among all the areas and the infected ratio in node 0 reaches its peak. In Figs. 2(c)–2(e), the infected population decreases and finally reaches zero, which is the stable state of the system.
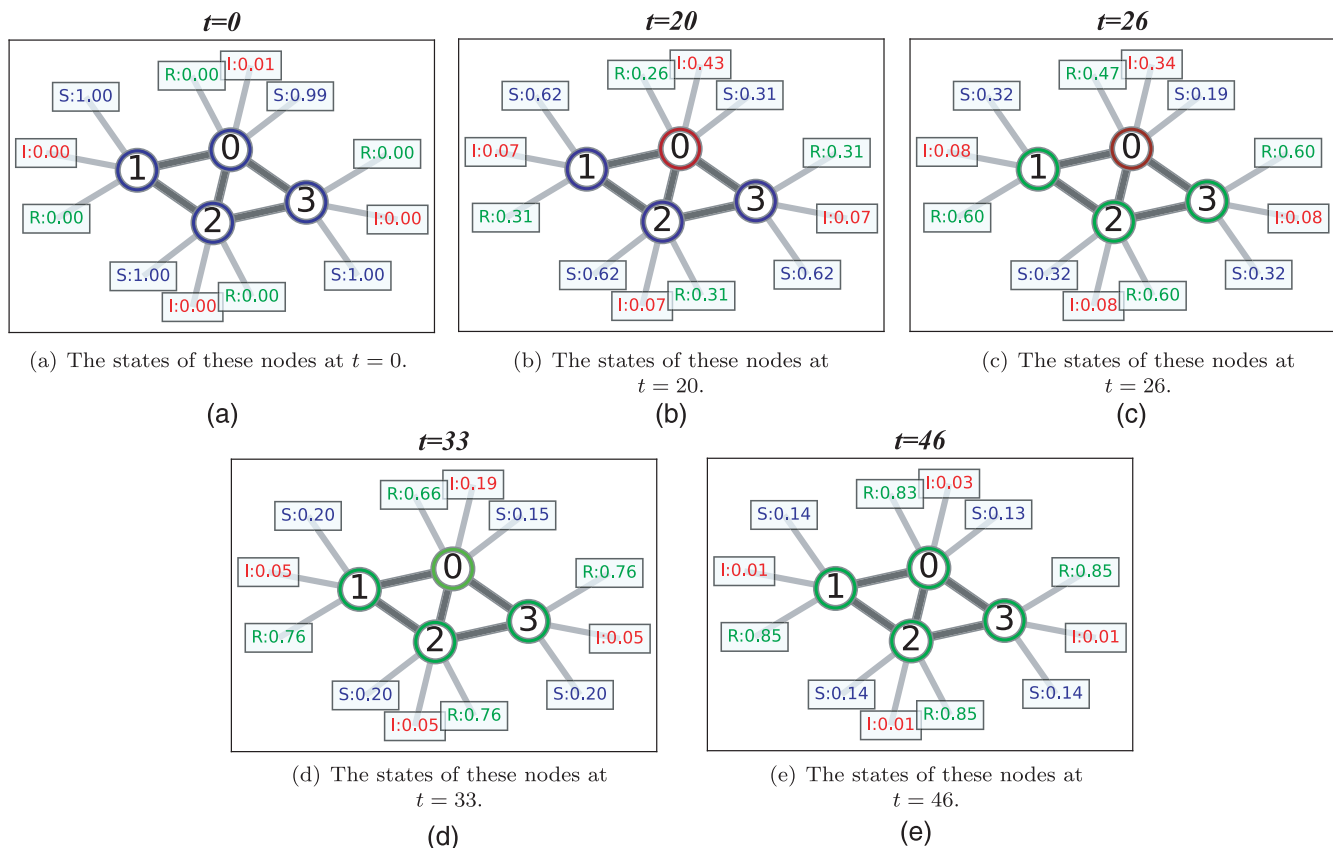
## III. SIMULATION

In this section, we mainly analyze the epidemic spreading process utilizing the proposed modeling process to generate a sequence of node states varying with time in a given network after the disease begins to spread. In Sec. III A, we study the state vector during the epidemic process, where the three epidemic states perform differently during the process and become stationary simultaneously after some time. In addition, to analyze the peak infected ratio of a node and the total infected ratio in the whole network, we analyze the influence of the infect transition rate $\beta$ and connection strength $\sigma$ in Sec. III B. Specifically, we utilize python to run all these simulations. We simulate the epidemic spreading process among individuals and areas on these common networks:

- WS small-world networks that randomly re-attach edges on a network where each node is connected with its k nearest neighbors. Adjusting the rewiring parameter $p$ makes it possible to interpolate between a regular lattice at $p = 0$ or a structure close to an Erdös–Rényi random graph at $p = 1$. To balance this, we set the $p = 0.5$.
- BA networks which follow the growth and preferential attachment principle. The BA network has hubs due to a preferential attachment mechanism. By analyzing it, we obtain the properties of spreading in area networks with hubs.
- Circulant graphs are undirected graphs act on by a cyclic group of symmetries that takes any vertex to any other vertex.[28] Circulant graphs stand for networks where the nodes have the same degree, and in circulant graphs, all the vertices have the same status.

Previous studies have shown that real-world regional networks have scale-free or small-world property; therefore, it is reasonable to utilize the BA network or WS network as the model of the area network. In contrast, due to the homogeneity of nodes in circulant graphs, we utilize simulation results on circulant graphs as a comparison. In our model, we set the networks to have dozens of nodes since the area as the basic unit should not be large. In addition, in the real world, due to epidemic prevention policy, the infected population usually has a lower migration rate than the uninfected population. Thus, we set the diagonal matrix **H** in the linear output function to be $(1, 0.01, 1)$, i.e., only a small amount of the infected population can move to other areas.

Based on the above preparations, we next present simulations of our epidemic model.

*t=0*

(a) The states of these nodes at $t = 0$.

(a)

*t=20*

(b) The states of these nodes at $t = 20$.

(b)

*t=26*

(c) The states of these nodes at $t = 26$.

(c)

*t=33*

(d) The states of these nodes at $t = 33$.

(d)

*t=46*

(e) The states of these nodes at $t = 46$.

(e)

**FIG. 2.** Epidemic spreading among four areas as nodes numbered 0, 1, 2, 3. The figure shows how the epidemic spreads among areas based on our model. The *S*, *I*, and *R* indicate the value of the three components of the state vector in each node, and the change of color shows the epidemic spreading process in this network. The epidemic first starts in node 0 and then spreads to other nodes. The values in the boxes connected to nodes indicate the state vector of nodes. (a) The states of these nodes at $t = 0$. (b) The states of these nodes at $t = 20$. (c) The states of these nodes at $t = 26$. (d) The states of these nodes at $t = 33$. (e) The states of these nodes at $t = 46$.

## A. Time variation analysis

In this subsection, we demonstrate the epidemic state of the state vector in each node in a given network, varying with time during the spreading process.

We generated a BA network with 16 nodes and the attachment parameter $m = 4$. Then, we select a node, set its initial $I$ nonzero, and let $S = 1 - I$, while all other nodes are all set as $I = 0$ and $S = 1$. The spreading parameter $\beta = 0.5$, and the recovery transition rate $\gamma = 0.2$ to ensure $\beta/\gamma > 1$, which guarantees the disease to spread around. In addition, we let the connection strength $\sigma = 0.3$ as a small value to avoid causing the vector state has negative components during the epidemic. Through these settings, we show the dynamic process of the three states of different nodes varying with time in Fig. 3.

In Fig. 3, we can see that the evolution of nodes following Eq. (1) and the process reaches the stable state in the end. In Figs. 3(a)–3(c), different lines represent different ratios of the population state in different nodes in the network, while in Figs. 3(d)–3(f), we focus on the difference between the node state

and the *average node state*, which describes the deviation of the node state to the whole group state.

Figures 3(a)–3(c) illustrate the dynamic process of states for each node. We finally obtain the synchronization of node states through their different evolutionary routes. In addition, the stable value of the recovered ratio in the node is 0.89, which is also the same value as the result of the SIR model, taking the same parameters $\beta = 0.5$ and $\gamma = 0.2$, suggesting that with an extra network structure, the outcome of the SIR model remains the same. Moreover, we can see that in Fig. 3(b), one of the nodes gets an extremely large infected ratio compared to the others at some time point, since it is the first node where the disease outbreaks, while the increase of the recovered population lowers the infected ratio in other nodes. In Figs. 3(d)–3(f), we introduced $\mathbf{e_i} = \mathbf{x_i} - \bar{\mathbf{x}}$, where $x_i$ is the state vector of nodes $i$ and $\bar{\mathbf{x}} = \frac{1}{N} \sum_i \mathbf{x_i}$, to measure the distance between the vector state of one node and that of the entire group. Each line is the process of the error rate of the state value during the period in the corresponding area. We can observe that all the components of each $\mathbf{e}_i$ of the corresponding node become 0, indicating that the state
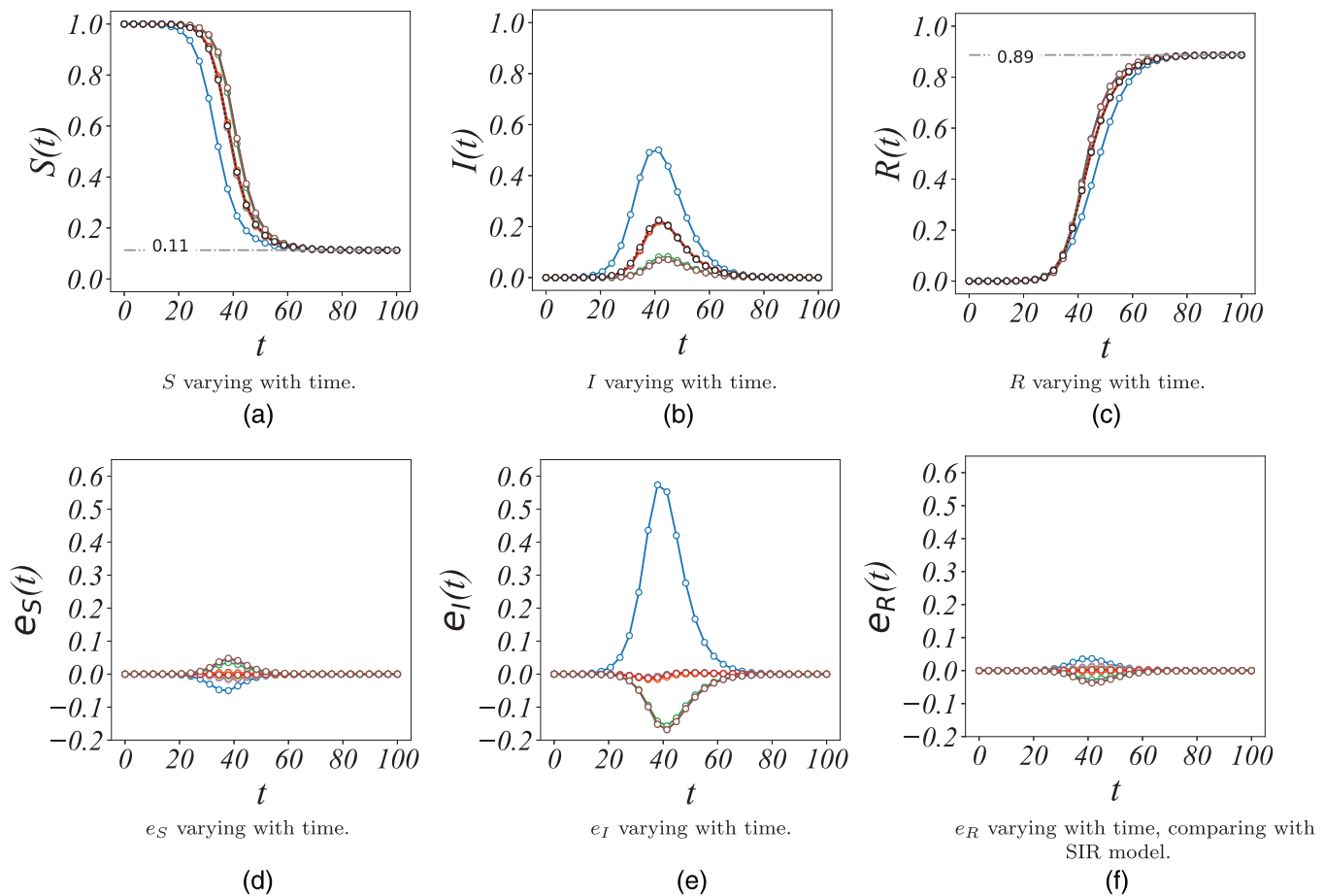
**FIG. 3.** The outcome of disease in a BA scale-free network that has 16 nodes and the attachment parameter $m = 4$. The parameters of the output function are $H_{11} = 1$, $H_{22} = 0.001$, and $H_{33} = 1$, which means the individuals in the susceptible class or recovered class can move from one area to another, and the infected can hardly move due to the illness. In addition, the coupling strength $\sigma = 0.3$, and the spreading parameters $\beta = 0.5$ and $\gamma = 0.2$. (a)–(c) show how the ratio of $S$, $I$, $R$ in population changes with time through the spreading dynamic model. In (d)–(f), for each node, we have $\mathbf{e_i} = \mathbf{x_i} - \bar{\mathbf{x}}$ and $\bar{\mathbf{x}} = \frac{1}{N} \sum_i \mathbf{x_i}$. 16 different lines are plotted; thus, we hide the legend. This shows the evolution of the difference between nodes. (a) $S$ varying with time. (b) $I$ varying with time. (c) $R$ varying with time. (d) $e_S$ varying with time. (e) $e_I$ varying with time. (f) $e_R$ varying with time, compared with SIR model.

is stable. In addition, the process shows an increase and decrease in state differences among nodes, and the $I$ state has the largest variance and fluctuates most greatly, which suggests during the whole epidemic period, the ratio of infected is quite different from node to node.

To compare the typical SIR model and our proposed model with area coupling, we apply both models and present the proportions of individuals in three epidemic states varying with time with two different models in Fig. 4. In our model, there are a number of areas, and we choose the area where the epidemic began to spread and a randomly chosen area for observation as well as the average value of all the areas. As we can see in Fig. 4(a), the proportion of susceptible individuals in our model begins to decrease later than that of the typical SIR model, and it also reaches a stationary state later than that of the typical SIR model with the same stationary value

below 0.2. From Fig. 4(b), the trends of the lines of our model and the types are the same, and all of them eventually become 0 when the system is stationary. However, the fraction of the infected of the typical SIR model peaks at $t = 30$ approximately, while the infected fractions in our proposed model all peak behind $t = 40$. In addition, the highest value of the average infected proportion of all the areas in our model is lower than that of the typical SIR model. As is shown in Fig. 4(c), recovered individuals in our model also increase later than that of the typical SIR model and reach the stationary state later compared to the typical SIR model. The stationary values for the recovered fraction are the same in both models. In conclusion, in simulations, the stationary fractions of susceptible and recovered individuals based on Eq. (1) are the same as those of the typical SIR ordinary differential equations (ODEs). While the peak value of the infected fraction based on Eq. (1) is different from that of the typical
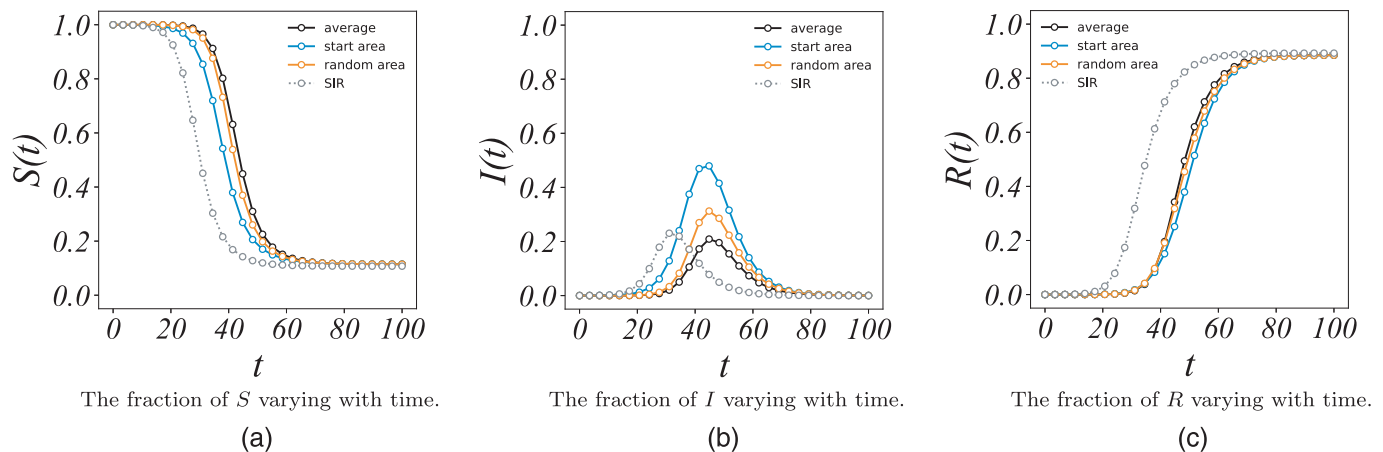
**FIG. 4.** The fractions of susceptible, infected, and recovered individuals varying with time are presented, respectively. Gray dashed lines indicate the fraction of individuals in three states based on the typical SIR ordinary differential equation, while solid lines represent the fraction of three states according to our proposed model in Eq. (1). We select the area where the disease first begins to spread marked by blue solid lines, a randomly chosen area with orange solid lines for observation. We also show the average value of all the areas marked by black solid lines for comparison. The stationary fraction of susceptible and recovered individuals in the two models are the same; however, the time when the system reaches stationary is different. The peak values of the fraction of infected individuals are also different in the two models. (a) The fraction of $S$ varying with time. (b) The fraction of $I$ varying with time. (c) The fraction of $R$ varying with time.

SIR ODEs due to the network coupling in our model, and there is divergence among different areas in terms of the peak infected ratio (PIR) and the time that the system reaches a stationary state.

To illustrate the effect of spatial factors on epidemic spreading, we can also compare the spreading process of different areas shown in Fig. 4. From Fig. 4(a), the proportion of susceptible individuals in the start area begins to decrease from 1 at the earliest, and the susceptible fraction in the area we randomly choose in the network decreases later. The susceptible fraction of the start area also reaches a stationary state earlier compared to the randomly chosen area. In addition, susceptible individuals in both areas decrease earlier than the average level. However, we can see that the stationary values of the susceptible proportion are the same. A similar situation can be seen in the proportion of recovered individuals shown in Fig. 4(c). In Fig. 4(b), the peak value of the infected proportion is the highest in the start area at about 0.5, and it is above 0.3 in the randomly chosen area. Both of the peak values in the two areas are higher than the average value. The time difference in the proportions in three states among areas is due to our model where the disease occurs originally in an area then it takes time to spread to other areas. In addition, the value of PIR varies in different areas in our model. Therefore, the coupling among areas that indicates the migration or transportation flows in our model contributes to spatial effects, i.e., differences in the epidemic outbreak time and the peak value of the infected fraction.

In Sec. III B, we analyze the infected ratio, which is related to both the network structure and disease properties.

## B. Peak infected ratio analysis

In this subsection, we focus on the peak infected ratio of different areas. From the simplified simulation results in the above section, the infected ratio of the node first increases and then decreases. A similar phenomenon can be found in the real world and is of significance in addressing the epidemic spreading, which leads to our analysis of the peak infected ratio of areas.

To simplify the notation, for the area network in Eq. (1), we define PIR to be a vector formed by the peak infected ratio of nodes and $PIR_j$ to be the peak infected ratio in node $j$ during the period.

$PIR_j$ depends on both the dynamic of node $j$ itself and the state of its neighbors. In particular, when there is only one node 0, our model simplifies into the SIR model not considering the epidemic spreading among areas. In this simple case, where only one node 0 exists simplifying the system into the SIR model, the PIR vector has only one component $PIR_0$ in the system and the peak infected ratio will be approached for $dI_0/dt = 0$ and $dR_0/dt > 0$. Hence, the turning point of the epidemic is the case that more people get recovered than get infected during the period.

The system with one area only considers its dynamic process and it is easy to figure out the numerical solution. However, considering the interaction between areas is more complicated, since the epidemic spreading is affected by the structure of the network, connection strength of the network of the node coupling, and the initially infected areas. Due to the complexity to obtain the influence of parameters in Eq. (1), we run a bunch of simulations to show the PIR varying with different parameters.

For each node denoted as $j$ in the network, we obtain a group of $PIR_j$ and mainly focus on the index *max*, *mean*, *min*, and *variance coefficient* of the data. The *max* is denoted as the maximum value of the infected ratio of the nodes during the whole time; hence, this index implies a high infected ratio in the area. However, *max* only covers the infected ratio in one area, ignoring the infected ratio in other areas. Hence, we also let *mean* be the average value of all the $PIR_j$ for each node $j$ in the network and *min* be the minimum

value of all the $PIR_j$ for each node $j$ in the network, which makes the description of the data more comprehensive. In addition, we introduce $c_v$ to be the variation coefficient defined as the variance divided by average and show the extent of variability to the mean value of the population.

For the interaction between areas, which is the node coupling in our model, $\sigma$ and $\mathbf{H}$ reflect the strength of the connection between two nodes. Concretely, $\sigma$ is the connection strength of all the epidemic states of the state vector, while $H_{11}$, $H_{22}$, and $H_{33}$ denote the connection strength of each component. However, the migration rate of the uninfected population has fewer influences on the result compared to the migration rate of the infected population. We, thus, only consider $\sigma$ and ignore the difference between the uninfected population migration in our analysis. Additionally, node properties and network structures have a great influence on the infected ratio, higher degree causes more interactions with other nodes, which means a stronger population migration to the area in practical, leading more likely to import infected population. In addition, the shorter average shortest path also speeds up the process that the infected population spreads among the whole network.

In the following part, we investigate the influence of different parameters on the epidemic spreading. We first analyze how the $PIR$ varies with the connection strength between nodes; then, analyze the effect of the $\beta$, which always causes a growing infected population, and next present a heatmap to show the results when both connection strength and infect transition rate vary.

We compare the simulation results in the three different networks, WS networks, BA networks, and circulant networks. We generate three WS networks with different average values of the degree that are $k_{WS} = 4, 8, 16$. We also generate three BA networks with different attachment parameters $m_{BA} = 4, 8, 16$. In addition, we generate three circulant networks with different average values of degree $k_{Cir} = 4, 8, 16$. These settings aim to generate different types of networks with different densities of edges.

The initial number of nodes in all networks is set as 100, and we let the infect transition rate $\beta = 0.5$, and the recovered rate $\gamma = 0.2$. Given a network, the epidemic starts at a node with the average degree and spreads around the network until the system reaches a stationary state in the end. We set the connection strength $\sigma$ in the range of $(0.05, 0.75)$ with an interval of $0.05$, and for each $\sigma$ we simulate the spreading process based on the given network and record the state vector of each node. In addition, we calculate the *max*, *mean*, *min*, and $c_v$ of the data, which is shown in Fig. 5, where we analyze how $PIR$ is related to $\sigma$ in different networks or in the same type of network with different parameters.

To illustrate the correlation of these data more rigorously, we utilize the Pearson correlation coefficient, which is the covariance of the two variables divided by the product of their standard deviations, as a normalized measurement of the covariance of two factors. The formula for the Pearson coefficient is

$$r = \frac{\sum (X_i - \bar{X})(Y_i - \bar{Y})}{\sqrt{\sum (X_i - \bar{X})}\sqrt{\sum (Y_i - \bar{Y})}},$$

where $X_i$ and $Y_i$ are the individual sample points indexed with $i$. The correlation coefficient ranges from $-1$ to $1$. A value of $+1$



(a)



(b)



(c)



(d)
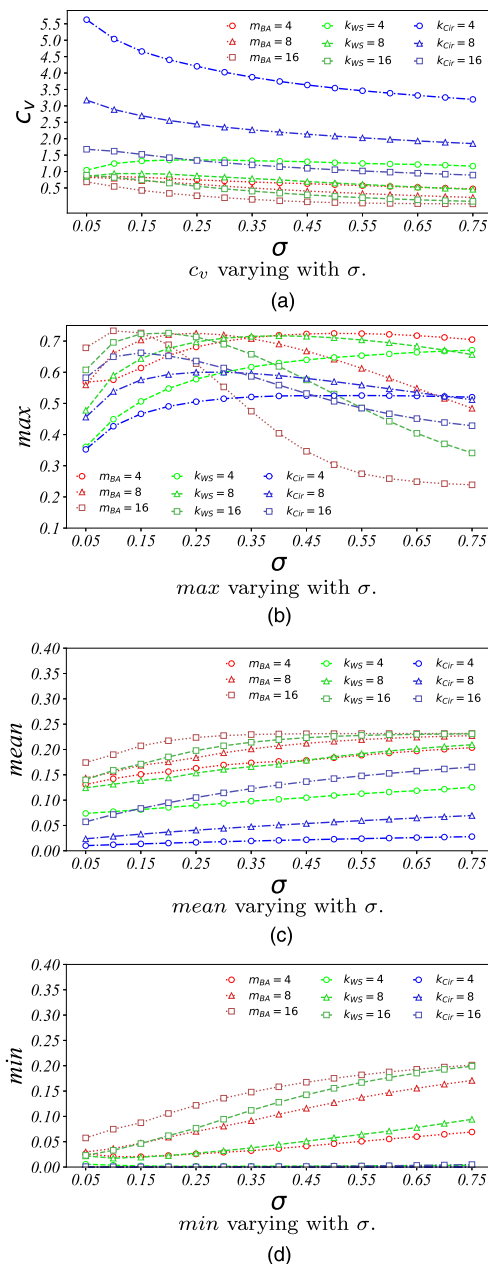
**FIG. 5.** The $c_v$, *max*, *mean*, and *min* of $PIR$ vary by $\sigma$ in different networks. The red, green, and red lines denote the simulation results of BA networks, WS networks, and Circulant networks. The markers on these lines, from circles, and triangles to squares, indicate the increase in degrees. From these figures, we show the effect of $\sigma$ on PIR in the three types of networks of different scales.

implies that all data points lie on a line for which $Y$ increases as $X$ increases and vice versa for $-1$. A value of $0$ implies that there is no linear dependency between the variables. The closer the absolute value of the Pearson coefficient is to one, the stronger the linear

**TABLE I.** The Pearson correlation coefficient of $\sigma$ with the *max*, *mean*, *min* and $c_v$ of *PIR* in different network structures.

|  | $c_v$ | *max* | *mean* | *min* |
|---|---|---|---|---|
| $m_{BA} = 4$ | −1.00 | 0.81 | 0.99 | 0.97 |
| $m_{BA} = 8$ | −0.99 | −0.65 | 0.96 | 1.00 |
| $m_{BA} = 16$ | −0.91 | −0.96 | 0.78 | 0.98 |
| $k_{WS} = 4$ | −0.18 | 0.89 | 1.00 | −0.10 |
| $k_{WS} = 8$ | −0.97 | 0.51 | 1.00 | 0.98 |
| $k_{WS} = 16$ | −0.98 | −0.90 | 0.91 | 0.99 |
| $k_{Cir} = 4$ | −0.94 | 0.74 | 1.00 | 0.46 |
| $k_{Cir} = 8$ | −0.96 | −0.11 | 0.99 | 0.91 |
| $k_{Cir} = 16$ | −0.98 | −0.93 | 0.98 | 0.88 |

correlation is; on the contrary, the closer the absolute value of the Pearson coefficient is, the weaker the linear correlation is. Utilizing the Pearson coefficient, theoretical analysis of the numerical results can be obtained. The Pearson correlation coefficient of $\sigma$ with these properties is calculated in Table I.

In Fig. 5(a), we illustrate the coefficient variance change for different network structures varying from the connection strength. It displays that, with a smaller degree, the slowing down of the epidemic spreading causes a higher variance among areas, especially for the circulant network, since it is featured with a longer average shortest path than the other two types of networks. The Pearson correlation coefficient shows a strong negative correlation in these networks.

In Fig. 5(b), we present the maximum of *PIR* change for different network structures varying with the connection strength $\sigma$. We can see that as $\sigma$ increases, it reduces the infected ratio decline in an area. The result seems to be counterintuitive; however, higher population migration reduces the infected ratio in an area with an infected ratio higher than the neighbors, i.e., more connections make neighbors share the stress of areas with a higher infected ratio. The Pearson correlation coefficient shows that the correlation of *max* and $\sigma$ seems to be uncertain in these networks. However, though the maximum infected ratio decreases, increasing the interaction can raise the average infected ratio.

In Fig. 5(c), we show how the average of *PIR* changes for different network structures varying from the connection strength. It shows that all the lines monotonically increase and the Pearson correlation coefficient shows a strong positive correlation, indicating that a higher $\sigma$ leads to a higher total infected ratio from the perspective of the whole network. In addition, in Fig. 5(d), we show how the min of *PIR* changes for different network structures varying from the connection strength, which has a similar result as in Fig. 5(c), and the Pearson correlation coefficient also shows a strong positive correlation.

Next, we present the influence of $\beta$. In the original work of Kermack and McKendrick, the final results of the epidemic depend on both the infection transition rate and the recovery transition rate, which means the outcome of the SIR model depends only on the rate of individuals infected and recovered. In our model, the final value of *PIR* can be figured out by solving Eq. (1). However, with different topological structures, the outbreaks of disease are also different.

When the epidemic inside the areas follows the SIR model, interacting with other areas should be taken into account as well. Given a fixed value of $\gamma$, the infected ratio increases as $\beta$ gets larger. In addition, the max *PIR* increases fast, while the mean *PIR* grows slowly, since a larger $\beta$ leads to more recovered population in the area, which moves to other areas, resulting in the restrain of infection in other areas and a slowing down of the increase of *PIR*.

With the increase of the infection transition rate, the infected ratio also increases. However, different network structures cause a difference of *PIR* in the statistical index. In different network structures, the minimum or average of *PIR* gets larger with the increase of $\beta$ at different speeds. Next, we build networks with the same parameters shown in Fig. 5. The connection strength is set as $\sigma = 0.3$, and the infect transition rate $\beta$ is set from 0.24 to 0.6. The results are shown in Fig. 6 and the Pearson correlation coefficient of $\sigma$ with these properties is calculated in Table II.

Figure 6(a) illustrates the coefficient variance change for different network structures varying from $\beta$, and the curves seem to be irregular and the Pearson correlation coefficient is also uncertain, while in Figs. 6(b) and 6(c), which show how the max and average of *PIR* changes for different network structures varying from $\beta$, we observe the index value increase with the increase of $\beta$, which is consistent with our intuitive cognition. In addition, the Pearson correlation coefficient also shows a strong relationship. Moreover, Fig. 6(d) displays the minimum infected ratio, where the trend of circulant networks with a small average degree has barely changed. It suggests that in a circulant network, the epidemic can hardly spread to certain areas regardless of the infection rate. Consequently, though higher $\beta$ causes a higher infected ratio in the whole system, there are some nodes in the network that have a low infected ratio.

A higher $\beta$ causes higher *max* and *mean* of *PIR* since higher infectivity of the disease causes more infected individuals leading each area to a large value of *PIR*. While a higher $\sigma$ results in a higher total infected ratio but have a possibility of lowering the *max PIR* among different areas, since more frequent population migrations may lead to infected individuals transferring among different areas, which balances the peak infected ratios of areas.

To understand the difference between them, we build a WS network with 50 nodes, 4 initial edges, and a rewire probability $p = 0.5$. We choose this network due to its small-world property, and by varying $p$, we can balance it between a regular and a random network. With the same network, we begin the epidemic simulation in a node with an average degree, and we vary $\sigma$ and $\beta$ in each experiment. To deeply understand the relationship among *PIR*, $\sigma$, and $\beta$, we run the simulation with the connection strength $\sigma$ ranging from 0.05 to 0.55 at an interval of 0.05 and set the infect transition rate $\beta$ ranges from 0.25 to 0.7 at an interval of 0.05, and the result is illustrated in Fig. 7.

In Fig. 7, we utilize heatmaps to show the result, in which the color of the grid shows the max/mean *PIR* value of the simulation with the different parameters. In Fig. 7(b), we observe that a higher $\beta$ or higher $\sigma$ causes a higher mean *PIR*. A higher $\sigma$ indicates a stronger connection among nodes, while a higher $\beta$ increases the infectivity of disease among the population. Though the property is different, the two parameters have on average a similar effect that their increase causes more infected population. In Fig. 7(a),
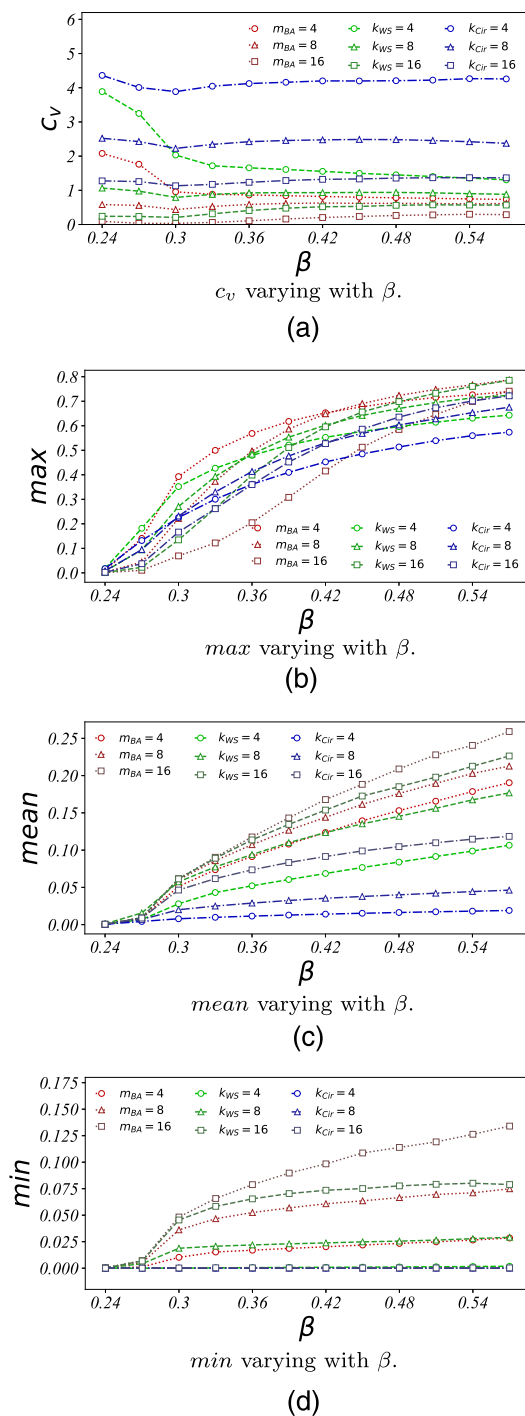
**FIG. 6.** The statistical indicators *max*, *mean*, *min*, and $c_v$ of *PIR* vary by $\beta$ in BA network with $m_{BA} = 4, 8, 16$, WS network with $k_{WS} = 4, 8, 16$, and the circulant network with $k_{Cir} = 4, 8, 16$. From these figures, we show the effect of $\beta$ on PIR in the three types of networks. (a) $c_v$ varying with $\beta$. (b) *max* varying with $\beta$. (c) *mean* varying with $\beta$. (d) *min* varying with $\beta$.

**TABLE II.** The Pearson correlation coefficient of $\beta$ with the $c_v$, *max*, *mean* and *min* of *PIR* in different network structures.

|              | $c_v$   | *max* | *mean* | *min* |
|--------------|---------|-------|--------|-------|
| $m_{BA} = 4$  | $-0.75$ | 0.89  | 0.99   | 0.95  |
| $m_{BA} = 8$  | 0.59    | 0.95  | 0.98   | 0.91  |
| $m_{BA} = 16$ | 0.95    | 0.99  | 0.99   | 0.96  |
| $k_{WS} = 4$  | $-0.80$ | 0.90  | 0.99   | 0.99  |
| $k_{WS} = 8$  | $-0.28$ | 0.94  | 0.98   | 0.86  |
| $k_{WS} = 16$ | 0.94    | 0.97  | 0.98   | 0.85  |
| $k_{Cir} = 4$ | 0.45    | 0.96  | 0.96   | 0.52  |
| $k_{Cir} = 8$ | 0.13    | 0.96  | 0.95   | 0.58  |
| $k_{Cir} = 16$| 0.79    | 0.98  | 0.95   | 0.56  |

however, when it comes to the max *PIR*, increasing $\sigma$ can hardly change the result and even reduces the value in some cases.

The enlightenment of this is, without a thorough isolated area, the population migration probably will not affect the result of the epidemic strongly, while rational measures to reduce the infect transition rate can be of great use.

## C. Real-world data

Due to the COVID-19 epidemic, we have data on the proportion of infected people in various cities in each country as a reference. In the following analysis, we apply our area spreading model to fit the real-world data of COVID-19. As for real-world data, we choose the statistical data set of COVID-19 for these three countries: the USA, China, and India (data sets from Novel Corona Virus 2019 Data set: https://www.kaggle.com/sudalairajkumar/novel-corona-virus-2019-data set/version/151, and we choose the data from before 07/01/2021).

In simulations, we consider a nation as a network with nodes considered as different areas in the country, and we select WS networks as the underlying network in our model since studies show that area networks have the small-world property. We simulate the epidemic spreading process of different areas of a country according to Eq. (1), and adjust the value of the coupling parameter $\sigma$ to set the connection level among areas to describe the spatial factor. The higher the value of $\sigma$, the stronger the connection among areas in the country, which means a large transport flow or migration of population among these areas. Based on the results of the epidemic spreading process we simulate, we calculate the PIR value of each area as our simulation results. For real data, we obtain data sets that include the daily number of infected individuals in states or provinces. These real data reflect spatial factors since there are transportation flows or population migration among areas in a country all the time during epidemics. Hence, we set an appropriate value for the connection strength $\sigma$ for describing the mobility and migration flows among different areas around the country. Then, we further obtain $PIR_j$ for each province or state $j$ in the country according to the real infected individual numbers. We rank the values of PIR of both the simulation and real-world data from low to high and compare them.

Max $PIR$ with different $\beta$s and $\sigma$s.

(a)



Mean $PIR$ with different $\beta$s and $\sigma$s.

(b)
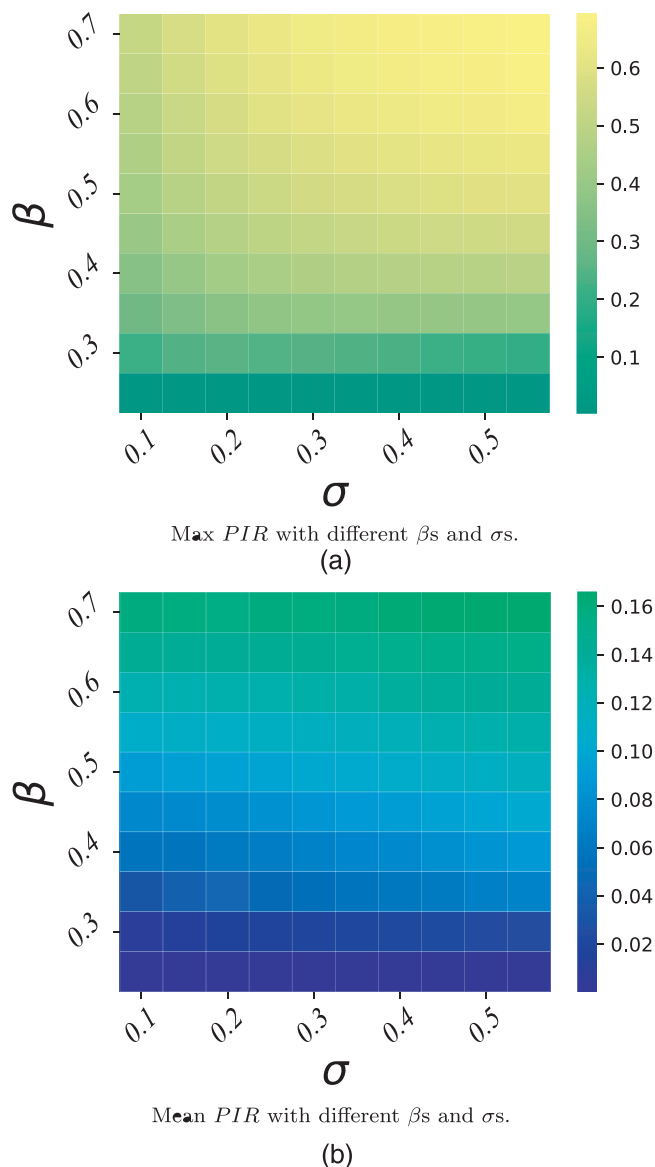
**FIG. 7.** The max and mean value of $PIR$ with two parameters $\beta$ and $\sigma$. The underlying network is a WS network with 50 nodes. The color of each grid indicates the value of the max or the mean of $PIR$ according to the color index. $\beta$ is set from 0.25 to 0.70, and $\sigma$ is set from 0.10 to 0.55. From the different appearances of these two figures, we obtain the different influences of the two variables on the $PIR$. (a) Max $PIR$ with different $\beta$s and $\sigma$s. (b) Mean $PIR$ with different $\beta$s and $\sigma$s.

The setting of the simulation applied to the real-world data is shown in Table III. The recovery rate is set to be the same for all the nations since we assume that there is no difference for individuals recovering from the same disease around the world. In addition, we set the connection strength $\sigma$ to be the same for all the networks. We set different infect transition rates $\beta$ for different

**TABLE III.** Parameters for the nations and the cross entropy between the $PIR$ distribution of our model and the real world. The small value of cross entropy shows the proximity of our model to the real world.

| Nation | USA | China | India |
|---|---|---|---|
| $n$ | 52 | 31 | 35 |
| $k$ | 10 | 4 | 5 |
| $\beta$ | 0.31 | 0.185 | 0.265 |
| $\gamma$ | 0.18 | 0.18 | 0.18 |
| $\sigma$ | 0.2 | 0.2 | 0.2 |
| Cross entropy | 2.356 | 0.350 | 1.316 |

countries according to the actual situation. For instance, as China has implemented a strict epidemic prevention strategy, and, thus, in our model, we set the model corresponding to China to have the lowest value of $\beta$ and the USA to have the highest value of $\beta$.

We also present the ratio of provinces or states with $PIR$ smaller than the given value to illustrate the $PIR$ distribution in each network. In the USA, all states experienced disease infection due to their relatively loose disease prevention and control. In contrast, due to the extremely strict epidemic prevention and control in China, the overall infection rate in China is relatively low and only one province China has a higher infection ratio than other areas. Compared with the first two, India is like a compromise of them. The simulation result and the real-world data are illustrated in Fig. 8.

In Fig. 8, on the left, we present the ranked $PIR$ of each area in the country and of the nodes in the corresponding network. On the right, we present the quantile on the distribution of the $PIR$ in both real data and simulation results, which show a great fit. In Fig. 8(a), we illustrate the real-world data and our simulation results of the USA, and most states in the USA have a high $PIR$. From the distribution of the $PIR_j$, we observe that about half of the areas have $PIR_j > 8\%$. In Fig. 8(b), we present the $PIR$ of China, and 97% of areas in China have a peak infected ratio $<0.1\%$, which is due to the strict epidemic prevention policy that leads to a low $\beta$. In Fig. 8(c), about half of the areas have a peak infected ratio lower than 2%, and the maximum is about 12%.

To measure the goodness of fitting for practical $PIR_j$ distribution based on the model we proposed, we utilize cross entropy as presented in Table III. By slightly changing the $\beta$, we obtain the illustrated results, which means the disease can be controlled by the decrease of $\beta$, suggesting that a strictly epidemic prevention strategy all over the network is of great use while restrained moving is probably useless if not being completely cut off.

However, to simplify the model, we assume that the population is continuous, which means that despite how strict the prevention and control are, there are always infected population migration into other areas, while it is not true in real world since discrete population makes no infected population migration becoming possible. Therefore, when migration can be completely forbidden, restrain moving in areas that have an infected population and carrying out strict epidemic prevention strategy in the areas is an economic strategy. On the other hand, even a single infected individual moving to other areas will cost great damage, so in this case, carried out an epidemic prevention strategy all over the country is more reasonable.
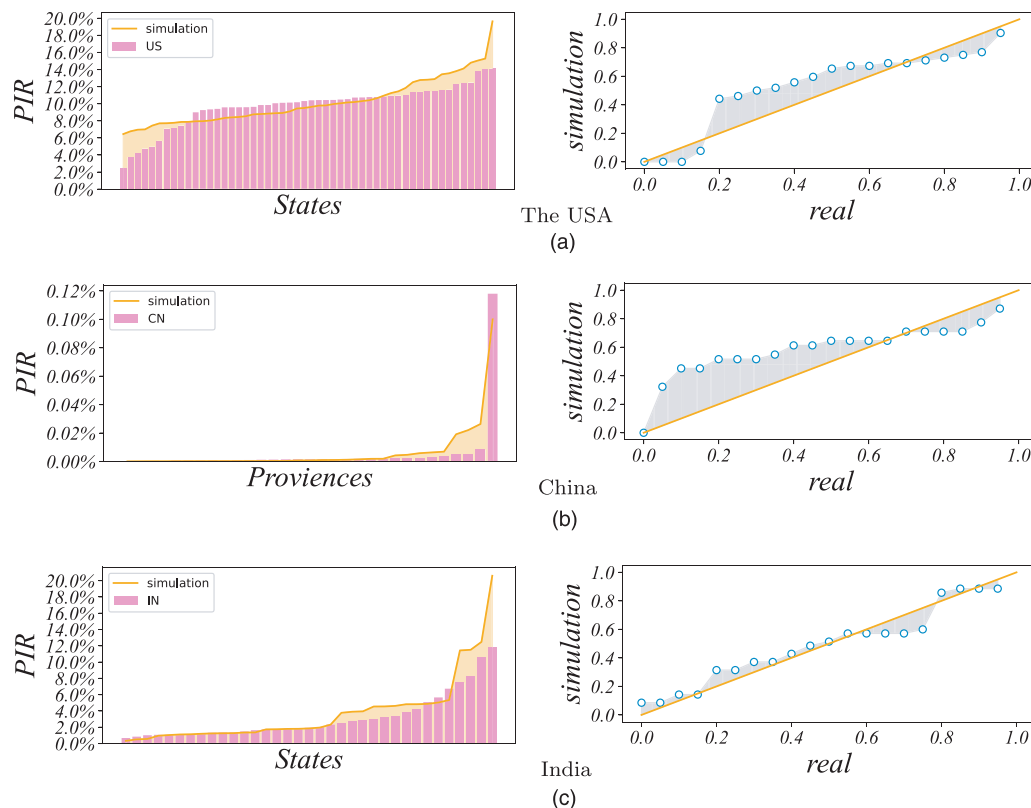
**FIG. 8.** By ranking the peak infected ratio during the time in each country in the nation, we illustrate the pink bars which denote the infected ratio, and the orange lines show the simulation results of the *PIR* in each node which is also sorted from low to high in Figs. 8(a), 8(b), and 8(c) on the left. On the right, each point $(x_i, y_i)$ the figure shows the quantile of the distribution. Each point stands for a certain *PIR* value, while $x_0$ and $y_0$ are corresponding to the quantile of the distribution of the real data and the simulation result. This gives a visual representation of the goodness of our model fitting real situations. (a) The USA, (b) China, and (c) India.

## IV. CONCLUSION

In this paper, to simplify the network spreading model when it comes to a system with different areas, we propose a model that regards areas as nodes in the network instead of the traditional model that considers individuals as nodes. With this new model, we analyze the maximum infected ratio in the system, which is not only affected by different topological structures of the network but also varies with both connection strength and the property of the disease. An increasing population movement between areas can relieve the pressure on the most infected areas to some extent, but it is likely to increase the proportion of infections in other areas. Reducing the infection rate in various areas over some time through a reasonable protection strategy can effectively reduce the highest infection rate. Finally, we conclude that the lockdown of an area can sometimes hardly work on lowering the infected ratio if not being completely isolated.

To simplify the process, our model is only based on a deterministic system. However, in future work, we will introduce a system with randomness to make our model more realistic. Then, there are other infectious disease dynamics models, e.g., SIS, SIRS, etc. that we have not implemented in this paper. The duration of the infected

ratio reaching a warning line also needs future study. All these issues will be our research goal for the next stage.

## ACKNOWLEDGMENTS

## AUTHOR DECLARATIONS

### Conflict of Interest

The authors have no conflicts to disclose.

### Author Contributions

**Qin Li:** Conceptualization (lead); Data curation (equal); Formal analysis (equal); Funding acquisition (lead); Investigation (equal); Methodology (lead); Project administration (equal); Writing – original draft (equal); Writing – review & editing (equal). **Hongkai Chen:** Conceptualization (equal); Data curation (equal); Formal analysis (equal); Methodology (equal); Software (lead); Writing –

original draft (lead). **Yuhan Li:** Conceptualization (equal); Data curation (equal); Formal analysis (equal); Investigation (equal); Methodology (equal); Resources (equal); Writing – review & editing (equal). **Minyu Feng:** Funding acquisition (lead); Methodology (equal); Project administration (equal); Supervision (equal); Writing – review & editing (equal). **Jürgen Kurths:** Funding acquisition (lead); Supervision (equal); Writing – review & editing (lead).

## DATA AVAILABILITY

The data that support the findings of this study are available from the corresponding author upon reasonable request.

## REFERENCES

[1] A. L. Bertozzi, E. Franco, G. Mohler, M. B. Short, and D. Sledge, "The challenges of modeling and forecasting the spread of COVID-19," Proc. Natl. Acad. Sci. U.S.A. **117**(29), 16732–16738 (2020).

[2] W. O. Kermack and A. G. McKendrick, "Contributions to the mathematical theory of epidemics, part I," Proc. R. Soc. Ser. A **115**, 700–721 (1927).

[3] W. O. Kermack and A. G. McKendrick, "Contributions to the mathematical theory of epidemics, part II," Proc. R. Soc. Ser. A **138**, 55–83 (1932).

[4] R. M. Anderson and R. M. May, *Infectious Diseases in Humans* (Oxford University Press, Oxford, 1992).

[5] R. Pastor-Satorras, C. Castellano, P. Van Mieghem, and A. Vespignani, "Epidemic processes in complex networks," Rev. Mod. Phys. **87**(3), 925 (2015).

[6] M. Newman, *Networks* (Oxford University Press, 2018).

[7] D. J. Watts and S. H. Strogatz, "Collective dynamics of 'small-world' networks," Nature **393**(6684), 440–442 (1998).

[8] A. L. Barabási and R. Albert, "Emergence of scaling in random networks," Science **286**(5439), 509–512 (1999).

[9] K. T. Eames, "Modelling disease spread through random and regular contacts in clustered populations," Theor. Popul. Biol. **73**(1), 104–111 (2008).

[10] S. C. Ferreira, C. Castellano, and R. Pastor-Satorras, "Epidemic thresholds of the susceptible-infected-susceptible model on networks: A comparison of numerical and theoretical results," Phys. Rev. E **86**(4), 041125 (2012).

[11] Y. Li, B. Pi, and M. Feng, "Limited resource network modeling and its opinion diffusion dynamics," Chaos **32**(4), 043108 (2022).

[12] Y. Li, Z. Zeng, M. Feng, and J. Kurths, "Protection degree and migration in the stochastic SIRS model: A queueing system perspective," IEEE Trans. Circuits Syst. I: Regul. Pap. **69**, 771–783 (2021).

[13] P. Van den Driessche and J. Watmough, "Reproduction numbers and sub-threshold endemic equilibria for compartmental models of disease transmission," Math. Biosci. **180**(1-2), 29–48 (2002).

[14] W. Wang and X. Q. Zhao, "An epidemic model in a patchy environment," Math. Biosci. **190**(1), 97–112 (2004).

[15] Y. Wang, Z. Wei, and J. Cao, "Epidemic dynamics of influenza-like diseases spreading in complex networks," Nonlinear Dyn. **101**(3), 1801–1820 (2020).

[16] V. Colizza, R. Pastor-Satorras, and A. Vespignani, "Reaction-diffusion processes and metapopulation models in heterogeneous networks," Nat. Phys. **3**(4), 276–282 (2007).

[17] V. Colizza and A. Vespignani, "Invasion threshold in heterogeneous metapopulation networks," Phys. Rev. Lett. **99**(14), 148701 (2007).

[18] A. Barrat, M. Barthelemy, R. Pastor-Satorras, and A. Vespignani, "The architecture of complex weighted networks," Proc. Natl. Acad. Sci. U.S.A. **101**(11), 3747–3752 (2004).

[19] S. Eubank, H. Guclu, V. S. Anil Kumar, M. V. Marathe, A. Srinivasan, Z. Toroczkai, and N. Wang, "Modelling disease outbreaks in realistic urban social networks," Nature **429**(6988), 180–184 (2004).

[20] W. S. Jung, F. Wang, and H. E. Stanley, "Gravity model in the Korean highway," Europhys. Lett. **81**(4), 48005 (2008).

[21] W. Li and X. Cai, "Empirical analysis of a scale-free railway network in China," Physica A **382**(2), 693–703 (2007).

[22] P. Sen, S. Dasgupta, A. Chatterjee, P. A. Sreeram, G. Mukherjee, and S. S. Manna, "Small-world properties of the Indian railway network," Phys. Rev. E **67**(3), 036106 (2003).

[23] A. Arenas, A. Diaz-Guilera, J. Kurths, Y. Moreno, and C. S. Zhou, "Synchronization in complex networks," Phys. Rep. Rev. Sect. Phys. Lett. **469**, 93–153 (2008).

[24] M. Barahona and L. M. Pecora, "Synchronization in small-world systems," Phys. Rev. Lett. **89**, 054101 (2002).

[25] L. M. Pecora and T. L. Carroll, "Master stability functions for synchronized coupled systems," Phys. Rev. Lett. **80**, 2109–2112 (1998).

[26] L. M. Pecora and M. Barahona, "Synchronization of oscillators in complex networks," Chaos Complexity Lett. **1**, 61 (2005).

[27] R. Olfati-Saber, J. A. Fax, and R. M. Murray, "Consensus and cooperation in networked multi-agent systems," Proc. IEEE **95**(1), 215–233 (2007).

[28] S. Radziszowski, "Small Ramsey numbers," Electron. J. Comb. (published online).